J. Fluid Mech. (1971), *vol.* 49, *part* 1, *pp.* 1–20
Printed in Great Britain

Generation of surf beat by non-linear wave interactions

By BRENT GALLAGHER
Department of Oceanography, University of Hawaii,
Honolulu, Hawaii 96822

(Received 19 October 1970 and in revised form 8 March 1971)

Non-linear interactions among wind-generated gravity waves transfer energy to low frequency waves in a coastal zone. A transfer function is derived for a straight coastline of constant bottom slope. This model is applied to three actual cases, and numerical evaluation of the energy transfer produces low frequency spectra which are compared with observations.

Introduction

In the late 1940's Munk and Tucker each independently discovered and recorded small amplitude, near-shore sea surface fluctuations in the frequency band between wind-generated waves and oceanic tides (10–40 cycles/1000 sec). These long-period oscillations, termed 'surf beat' by Munk, seemed related to the wind-generated waves incident upon the coast. Munk (1949) and Tucker (1950) both noticed a linear correspondence between wind-generated and surf-beat wave amplitudes, and Tucker found that the long-wave troughs correlated with wind-generated wave group crests. However, a causative physical connexion between the two types of waves was not understood. Our aim here is to demonstrate that non-linear interactions among wind-generated waves can excite coastal edge waves in the surf-beat frequency range and to illustrate that observed surf-beat energy levels might be accounted for by this process.

Investigations in non-linear water-wave theory suggest a mechanism for the inter-frequency energy transfer which seems involved in surf-beat generation. Commonly the full non-linear wave equations are approached with perturbation expansions; interactions among waves of a particular perturbation order then produce a transfer of energy to waves of higher order. The general method is demonstrated by Hasselmann (1961, 1963*a*, *b*). Potentially relating somewhat more specifically to surf beat, the work of Biesel (1952) showed that a long small-amplitude (second-order) undulation accompanies a first-order wave group. The second-order wave is forced, having the length and frequency of the group and not of a free, gravity wave – and it is 180° out of phase with the group in agreement with Tucker's observations. Similar results were obtained by Longuet-Higgins & Stewart (1962) who formulated the second-order effects in terms of the momentum flux associated with the propagation of first-order waves. This formulation leads to a physical interpretation of the long wave generation, which Longuet-Higgins & Stewart (1964) give. In regions of high waves the associated mass transport is greater than where the waves are low. Because of this difference in momentum

flux, fluid tends to be expelled from the regions corresponding to group crests and piled up in the group troughs – creating a second-order, long wave moving with the group. In the same paper, it is suggested that at the coast the swell is destroyed by breaking and the associated long wave is reflected seaward as a free wave.

In the present work, we extend the above ideas and examine quantitatively how a coastal region will respond to excitation produced by non-linear interactions among incident swell. The incident wind-generated waves are taken as the first-order solution in a perturbation expansion of the wave equations, and the surf beat is computed as the second-order low frequency solution. A transfer function is derived relating the surf-beat spectrum to the spectrum of incident swell, and numerical comparisons with observations are made.

Derivation of response spectrum

We use a model coastline which is straight and infinitely long, with the ocean bottom sloping downward offshore at a constant rate. An expression is constructed to represent the first-order incident wind-generated waves, and this is used to put the second-order wave equation in explicit form. Assuming the second-order response is sinusoidal along the coast, we obtain an inhomogeneous Laguerre equation whose solution leads to the surf-beat spectrum.

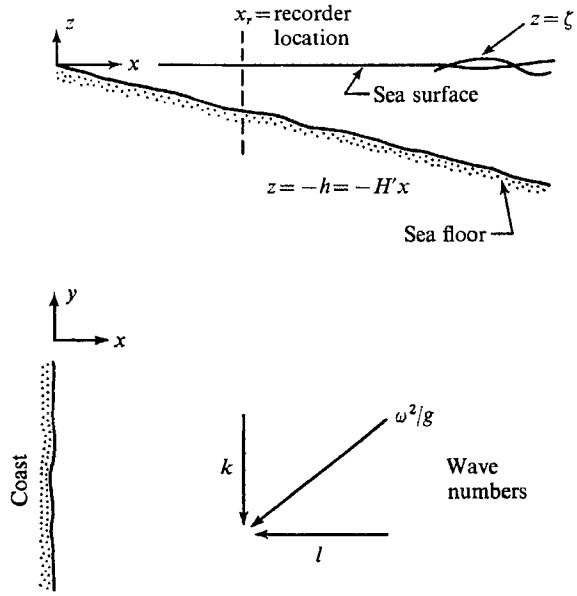

FIGURE 1. Coastal model and notation.

We assume a perfect incompressible fluid, so that perturbation expansions of the governing equations lead to relations describing Airy waves. We assume further that: (*a*) Incident wind-generated waves are totally destroyed at the shoreline, while low frequency waves are perfectly reflected. This, together with

the assumption below about incident wave amplitudes, means we are asserting that processes inside the surf zone may be neglected; in effect, the shoreline is placed at the outer edge of that region. (*b*) Incident wind-generated waves do not change wavelength as they shoal, and their amplitudes grow exponentially towards shore. This is only a crude description of shoaling waves. However, we feel the physics of the non-linear interactions will not depend strongly on the exact details of the wave forms and have chosen this description to simplify the mathematics. (*c*) In the first-order linear approximation, the wind-generated waves are statistically independent. This assumption is commonly taken in perturbation analysis of non-linear ocean waves; Hasselmann (1961) discusses a possible statistical justification for doing so. (*d*) Shallow-water, or long-wave equations will give an adequate description of the surf-beat waves in the coastal region. (Wavelengths are of order 1 km, and depths of order 10–100 m.) (*e*) Linear bottom friction will be adequate to simulate energy losses from the second-order waves. In the real world, edge wave energy is lost through bottom friction and by scattering to the open ocean induced by irregular topography. Linear friction correctly represents the mechanism of neither; it is merely a mathematically convenient way to remove an equivalent amount of energy from the coastal zone.

We express the velocity potential of the incident wind waves as a Fourier–Stieltjes expansion in frequency, ω, and long-shore wave-number k. The co-ordinate system and remaining notation are defined in figure 1.

$$\phi(x, y, t) = \int_{k=-\infty}^{\infty} \int_{\omega=-\infty}^{\infty} \tfrac{1}{2} d\phi(x, k, \omega) e^{i(ky-\omega t)}, \tag{1a}$$

$d\phi$ is related to spectral intensity, F, by

$$\tfrac{1}{2} \langle d\phi \overline{d\phi} \rangle = F(x, k, \omega) dk\, d\omega,$$

where $\langle\ \rangle$ indicates ensemble averaging, and the overbar denotes a complex conjugate. Because ϕ is real, $d\phi(k, \omega) = \overline{d\phi}(-k, -\omega)$.

Surface elevation is expressed in similar fashion

$$\zeta(x, y, t) = \int_{k=-\infty}^{\infty} \int_{\omega=-\infty}^{\infty} \tfrac{1}{2} dZ(x, k, \omega) e^{i(ky-\omega t)}, \tag{1b}$$

and we may convert surface elevation spectra to velocity potential spectra by using the linearized surface boundary condition, $g\zeta + \phi_t = 0$:

$$\langle d\phi \overline{d\phi} \rangle = (g^2/\omega^2) \langle dZ \overline{dZ} \rangle.$$

Under our assumptions, the first-order Fourier–Stieltjes amplitudes will depend on offshore distance as follows:

$$d\phi(x, k, \omega) = d\phi(k, \omega) . f(x, k, \omega) = d\phi(k, \omega) e^{-\alpha(x-x_r) - i \operatorname{sgn}(\omega) l x}.$$

x_r is the wave recorder location, α a parameter of order one, and l, the x component of the wave vector, is obtained from the deep-water dispersion relation $l^2 = \omega^4/g^2 - k^2$.

Perturbation expansions of the irrotational wave equations are derived in standard references such as Stoker (1957). To second order in a small parameter, such as sea-surface slope, these are

$$\nabla^2\phi^{(2)} = 0,$$

$$g\zeta^{(2)} + \phi_t^{(2)} = -\tfrac{1}{2}[(\phi_x^{(1)})^2 + (\phi_y^{(1)})^2 + (\phi_z^{(1)})^2] - \zeta^{(1)}\phi_{tz}^{(1)}, \quad \text{at} \quad z = 0,$$

$$\zeta_t^{(2)} - \phi_z^{(2)} = -\phi_x^{(1)}\zeta_x^{(1)} + \phi_{zz}^{(1)}\zeta^{(1)} - \phi_y^{(1)}\zeta_y^{(1)}, \quad \text{at} \quad z = 0,$$

$$\phi_z^{(2)} = -H'\phi_x^{(1)}, \quad \text{at} \quad z = -h = -H'x.$$

Superscripts refer to the order of the variable in the perturbation expansion. First-order expressions for the incident waves have been given above, and the second-order solution, representing surf beat, is now sought. Combining the surface boundary conditions, using the shallow-water assumption, and inserting a linear friction term in the resulting wave equation, we obtain:

$$\begin{aligned}\phi_{tt}^{(2)} + \epsilon\phi_t^{(2)} - (gh\phi_x^{(2)})_x - (gh\phi_y^{(2)})_y &= \frac{\partial}{\partial t}\{-\tfrac{1}{2}[(\phi_x^{(1)})^2 + (\phi_y^{(1)})^2 + (\phi_z^{(1)})^2] - \zeta^{(1)}\phi_{tz}^{(1)}\}_{z=0} \\ &\quad + g[\phi_x^{(1)}\zeta_x^{(1)} + \phi_y^{(1)}\zeta_y^{(1)} - \phi_{zz}^{(1)}\zeta^{(1)}]_{z=0} \\ &\equiv P(x, y, t), \end{aligned} \tag{2}$$

where ϵ is the linear friction coefficient.
Using the first-order solutions,

$$\begin{aligned}P(x, y, t) = \int_{k'}\int_{k''}\int_{\omega'}\int_{\omega''} &\left\{\frac{i(\omega' - \omega'')}{8}\left[\frac{f_x'\bar{f}_x''}{f'\bar{f}''} + k'k'' + \frac{\omega'^2\omega''^2}{g^2} - \frac{2\omega'\omega''^3}{g^2}\right]\right. \\ &\left. + \frac{i\omega''}{4}\left[\frac{-f_x'\bar{f}_x''}{f'\bar{f}''} - k'k'' + k'^2 - \frac{f_{xx}'}{f'}\right]\right\} d\phi(x, k', \omega')\, d\bar{\phi}(x, k', \omega'') \\ &\times e^{i[(k'-k'')y - (\omega'-\omega'')t]},\end{aligned}$$

where $f_x' = \partial f(x, k', \omega')/\partial x$, etc., and to shorten ensuing expressions we write

$$\begin{aligned}P(x, y, t) \equiv \int_{k'}\int_{k}\int_{\omega'}\int_{\omega''} &q(x, k', k' - k, \omega', \omega' - \omega) \\ &\times d\phi(x, k', \omega')\, d\bar{\phi}(x, k' - k, \omega' - \omega)\, e^{i(ky - \omega t)}.\end{aligned}$$

Here $k \equiv k' - k''$, $\omega \equiv \omega' - \omega''$, and these definitions apply throughout the remainder of this section.

To find $\phi^{(2)}$, we again expand:

$$\phi^{(2)}(x, y, t) = \int_k \int_\omega \tfrac{1}{2} d\phi^{(2)}(x, k, \omega)\, e^{i(ky - \omega t)}.$$

With the constant bottom slope H', and the abbreviation $d\phi = d\phi^{(2)}(x, k, \omega)$, equation (2) becomes:

$$\begin{aligned}x\, d\phi_{xx} + d\phi_x &= xk^2 d\phi + \frac{1}{gH'}\omega^2 d\phi + \frac{i\epsilon\omega}{gH'} d\phi \\ &= \frac{-2}{gH'}\int_{k'}\int_{\omega'} q(x, k', k' - k, \omega', \omega' - \omega)\, d\phi(x, k', \omega')\, d\bar{\phi}(x, k' - k, \omega' - \omega).\end{aligned} \tag{3}$$

Since this equation is linear we solve with one (k', ω')-component of the driving function and then integrate the result.

To get a convenient form of (3), substitute $z = 2|k|x$ and $d\psi = e^{-\frac{1}{2}z} d\phi$; a Laguerre equation results:

$$z\,d\psi_{zz} + (1-z)\,d\psi_z - \left[\frac{1}{2} - \frac{\omega^2 + i\epsilon\omega}{2gH'|k|}\right] d\psi = \frac{-e^{\frac{1}{2}z}}{gH'|k|}\, q\left(\frac{z}{2|k|}, k', k'-k, \omega', \omega'-\omega\right)$$

$$f\left(\frac{z}{2|k|}, k', \omega'\right) \bar{f}\left(\frac{z}{2|k|}, k'-k, \omega'-\omega\right) d\phi(k', \omega')\, d\bar{\phi}(k'-k, \omega'-\omega)$$

$$\equiv p\, d\phi(k', \omega')\, d\bar{\phi}(k'-k, \omega'-\omega).$$

A solution may be expressed in terms of Laguerre polynomials, $L_n(z)$.
Let

$$d\psi = \sum_{n=0}^{\infty} A_n L_n(z)$$

and

$$p\, d\phi\, d\bar{\phi} = \sum_{n=0}^{\infty} B_n L_n(z),$$

where n is integer and

$$A_n = \frac{1}{(n!)^2} \int_0^{\infty} e^{-z} d\psi(z)\, L_n(z)\, dz,$$

$$B_n = \frac{1}{(n!)^2} \int_0^{\infty} e^{-z} p(z)\, d\phi\, d\bar{\phi} L_n(z)\, dz.$$

Substitution in the equation gives

$$A_n = B_n \Big/ \left[n + \tfrac{1}{2} - \frac{\omega^2 + i\epsilon\omega}{2gH'|k|}\right],$$

where we have used the fact that $zL_{nzz} + (1-z)L_{nz} + nL_n = 0$, along with the orthogonality of the L_n's.

Working back through the substitutions made above, one obtains the solution to (3):

$$d\phi(x, k, \omega) = \int_{k'} \int_{\omega'} \left\{ e^{-|k|x} \sum_n \frac{I_n}{D_n} L_n(2|k|x) \right\} d\phi(k', \omega')\, d\bar{\phi}(k'-k, \omega'-\omega),$$

in which

$$I_n = \int_0^{\infty} e^{-\frac{1}{2}z} q\left(\frac{z}{2|k|}, k', k'-k, \omega', \omega'-\omega\right)$$

$$\times f\left(\frac{z}{2|k|}, k', \omega'\right) \bar{f}\left(\frac{z}{2|k|}, k'-k, \omega'-\omega\right) L_n(z)\, dz$$

and

$$D_n = (n!)^2 [(2n+1) gH'|k| - \omega^2 - i\epsilon\omega].$$

Computing a spectrum,

$$2F(k, \omega)\, dk\, d\omega = \langle d\phi(k, \omega)\, d\bar{\phi}(k, \omega) \rangle$$

$$= \left\langle \int_{k_1'} \int_{\omega_1'} T'(k, k_1'-k, \omega, \omega_1'-\omega)\, d\phi(k_1', \omega_1')\, d\bar{\phi}(k_1'-k, \omega_1'-\omega) \right.$$

$$\left. \times \int_{k_2'} \int_{\omega_2'} T'(-k, k_2'+k, \omega, \omega_2'+\omega)\, d\phi(k_2', \omega_2')\, d\bar{\phi}(k_2'-k, \omega_2'-\omega) \right\rangle$$

where T stands for the integrand in brackets { } above. Under the assumption that the wind-generated waves have statistically independent Fourier–Stieltjes amplitudes, the only non-zero terms in the above product occur when $k_1' = -k_2'$ and $\omega_1' = -\omega_2'$. Dropping the subscripts,

$$2F(k,\omega)\,dk\,d\omega = \int_{k'=-\infty}^{\infty}\int_{\omega'=-\infty}^{\infty} 4T\bar{T}F(k',\omega')F(k'-k,\omega'-\omega)\,dk'\,d\omega'\,d(k'-k)\,d(\omega'-\omega).$$

When the above integral is evaluated, it is necessary that $dk = d(k'-k)$ and $d\omega = d(\omega'-\omega)$ in order that each wind-wave spectral element contribute once and only once to the surf-beat spectrum. Furthermore, we must integrate $F(k,\omega)$ over k to get a result for comparison with observed non-directional long wave spectra. Then

$$F(\omega) = \int_{k=-\infty}^{\infty}\int_{k'=-\infty}^{\infty}\int_{\omega'=-\infty}^{\infty} 2T\bar{T}F(k',\omega')F(k'-k,\omega'-\omega)\,dk'\,d\omega'\,dk. \tag{4}$$

This is the final result; T is given by

$$T = e^{-|k|x}\sum_n \left\{\left[\int_0^\infty e^{-\frac{1}{2}z} q\left(\frac{z}{2|k|}, k', k'-k, \omega', \omega'-\omega\right) f\left(\frac{z}{2|k|}, k', \omega'\right)\right.\right.$$
$$\left.\left.\times \bar{f}\left(\frac{z}{2|k|}, k'-k, \omega-\omega\right) L_n(z)\,dz\right] L_n(2|k|x) \Big/ \left[n!^2((2n+1)gH'|k| - \omega^2 - i\epsilon\omega)\right]\right\}.$$

In the introduction, the idea was discussed that a long, low-amplitude, sea surface depression accompanies a group crest in wind-generated swell. The above analysis may be pictured in similar terms. In (4), each pair of incident swell trains, (k',ω') and $(k'-k,\ \omega'-\omega)$, may be thought of as a 'group' which contributes one particular low amplitude wave, (k,ω), to the total second-order response. Since k and ω are independent variables, most of these second-order waves do not obey a free wave dispersion relation and simply remain forced – dependent on the existence of the swell groups which create them. However, there are some combinations of k and ω in the driving function which do coincide with those of free waves in the coastal zone, and resonances occur. In the model used here, the free waves are edge waves, sinusoidal along shore, with offshore dependence described by Laguerre functions. Various modes of oscillation are specified by the index, n, of the Laguerre polynomials, and the appropriate frictionless, dispersion relation would be $\omega^2 = (2n+1)gH'|k|$.

Model parameters and their effects

Low frequency second-order response spectra are found through numerical evaluation of expression (4). We must provide a directional spectrum of incident wind-generated waves, as well as values for the bottom slope, the wave-recorder location, the exponential rate at which incident wave amplitudes grow toward shore, and the linear friction coefficient. The methods used in specifying these items, and the effects of varying the parameters are now discussed.

Directionality of incident waves

The non-linear interaction of waves incident from different directions is important in the second-order coastal response, but directional information is not usually provided by the observations. To overcome this, we assume that the wind-generated waves arrive from some base direction determined by the storm location, and that these waves are spread statistically around the base direction in a 'beam'. With the base longshore wave-number k_0, and a beam wave-number-width $2K$, we take

$$F(\omega, k) = F(\omega) . \frac{1}{K} \cos^2 \frac{\pi}{2K} (k - k_0), \; |k - k_0| \leqslant K$$

$$= 0, \; |k - k_0| > K.$$

Increasing the angle θ, between the incident wave direction and the coastal normal, produces greater energy at higher surf-beat frequencies. This is because of an increase in the number of pairs of incident wave components that can interact in resonance with coastal edge waves. Figures 2 and 3 show schematic, incident wave spectra contoured in the ω, k plane for two values of θ. The component located at (X) may interact with any other in the beam, but for resonance to occur this second component also must lie on one of the family of parabolas corresponding to edge wave dispersion relations: $(2n+1)gH'|k| = \omega^2$. It is apparent from the diagrams that for larger values of θ the intersection of an edge wave dispersion curve with the incident wave beam will be more extensive and will include higher edge wave frequencies. For the same reason, an increase in the incident wave beam width, β, also causes more excitation of the higher frequency edge waves, or surf beat. Sample computations showing these effects of beam direction and width on the response spectrum are shown in figure 4 (*e*) and (*f*).

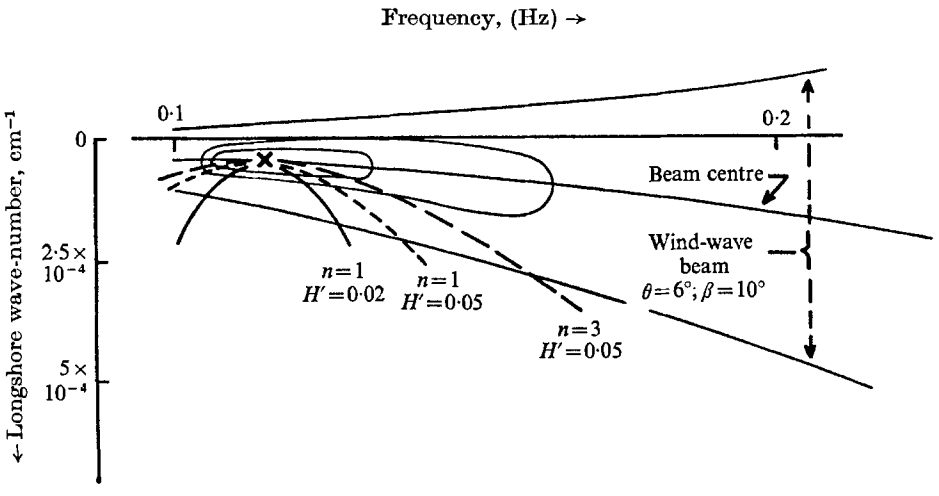

FIGURE 2. Schematic incident wave spectrum and edge wave dispersion relations in the ω, k plane.

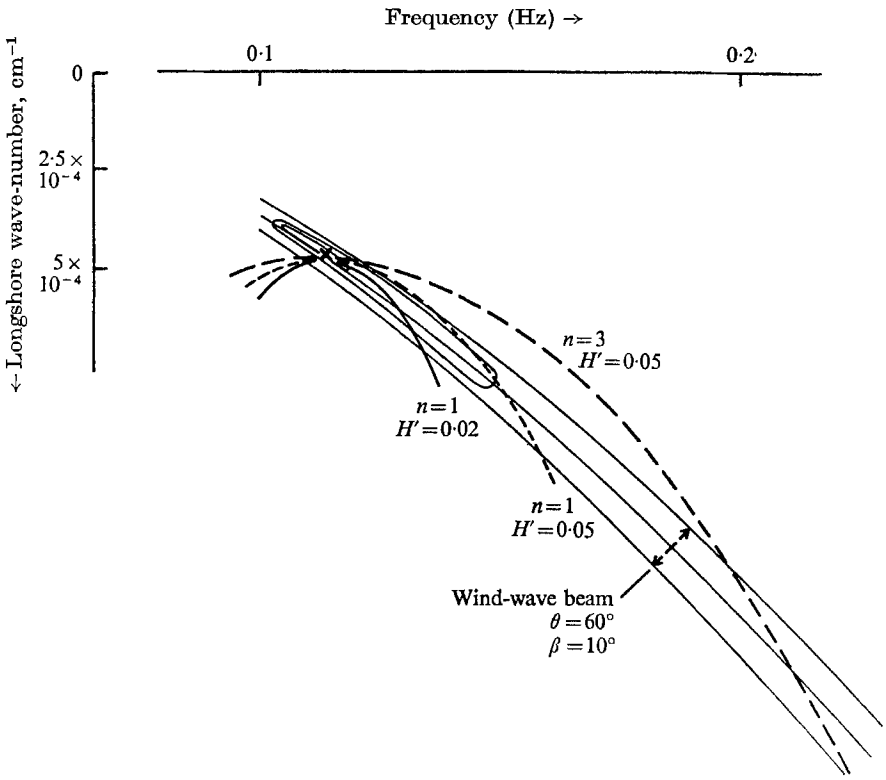

FIGURE 3. Schematic incident wave spectrum and edge wave dispersion relations in the ω, k plane.

Bottom slope

Bottom slope affects the response spectrum in two ways, each having the result that steeper bottoms favour the higher frequency surf-beat components. First, the slope influences the number of incident wave pairs that can resonate with a given edge wave mode and frequency. This can be seen in the ω, k diagrams of figures 2 and 3, where first-mode edge wave dispersion curves are drawn for two different slopes. Within the range of realistic slopes ($H' = 0{\cdot}01 - 0{\cdot}10$, say) the dispersion relations and incident wave beams will intersect more extensively and at higher frequencies as bottom slope is increased. Secondly, coastal edge wave energy decreases with distance offshore like $L_n^{2)}$, as seen in equation (4). These functions have exponential envelopes, $e^{-2|k|x}$; using the dispersion relation, we see that at any given distance offshore, such as at the recorder location, this envelope becomes proportional to $e^{-\omega^2/H'}$. Thus with steeper bottom slopes surf-beat energy is less strongly frequency-attenuated at any particular spot. This second result of slope compliments the first, and the combined effects on an example response spectrum are shown in figure 4(*a*).

To apply the model to actual coasts it is necessary to assign a single bottom slope somehow equivalent to the multiple slopes usually found in reality. In specific cases to be discussed shortly, the bottom sloped quite gradually away from the beach and then more rapidly offshore, with a rather definite break.

Experience showed that an average of the two gradients was a good first approximation to assign in the model.

Recorder location

x_r is the distance outside the breakers (the assumed shoreline) at which wind-wave and surf-beat spectra are actually measured, and at which the computed second-order spectrum is to be evaluated. Decreasing x_r shifts computed surf-beat energy toward higher frequencies. This is predictable from the form of the Laguerre functions together with the edge wave dispersion relation. Edge wave amplitudes decrease away from shore according to $L_n(2|k|x)$. If we shift the evaluation point, $x = x_r$, closer to shore, then any particular edge wave amplitude will be associated with a larger longshore wave-number and hence with higher frequency. Figure 4(*b*) shows this effect in an example computation.

Assigning x_r involves problems when the model is applied to field observations; a stationary straight line must be used to represent the outer edge of the surf zone. In reality this boundary can undergo temporal excursions in response to tides and to changes in swell conditions, and furthermore, actual 'straight' coastlines are not perfectly so. Thus we must choose an 'effective' x_r. A physically reasonable distance which gives the model predictive value would be 'effective', and we have been able to make such assignments in the cases studied.

Incident wave amplitude exponent

The amplitude of incident waves was taken to increase shoreward as

$$\exp(-\alpha(x-x_r)).$$

The shoreward steepness and amplitude of the second-order excitation will therefore increase as α is made larger, favouring the higher frequency edge wave responses, which have corresponding larger shoreward steepness. This anticipated effect is seen in figure 4(*d*).

We expect intuitively that the amplification of shoaling, incident waves may be more pronounced when their frequency spectrum is narrow. Thus, in a computation involving incident swell from a distant storm we chose α by assuming that the shoreline wave heights were three times greater than at 100 m offshore. In two cases where a broad spectrum of incident waves was provided by a nearby storm, α was taken as zero.

Friction coefficient

The linear dissipation parameter, ϵ, is adjusted empirically to obtain agreement between computed and observed surf-beat energy levels at a given location. Values in the range $10^{-6} - 10^{-5}\,\mathrm{sec}^{-1}$ produce the best results, and at this dissipation level, the resonant free edge waves contribute virtually all of the observed surf-beat energy. Then low frequency energy density is proportional to ϵ^{-2}, as shown in the example computations of figure 4(*c*).

The need for an empirically determined dissipation parameter is unfortunate; independent checks are required before full confidence can be placed in computed energy levels. We can present two such checks now and point out where further investigation is needed. First of all, ϵ, which is intended to represent both

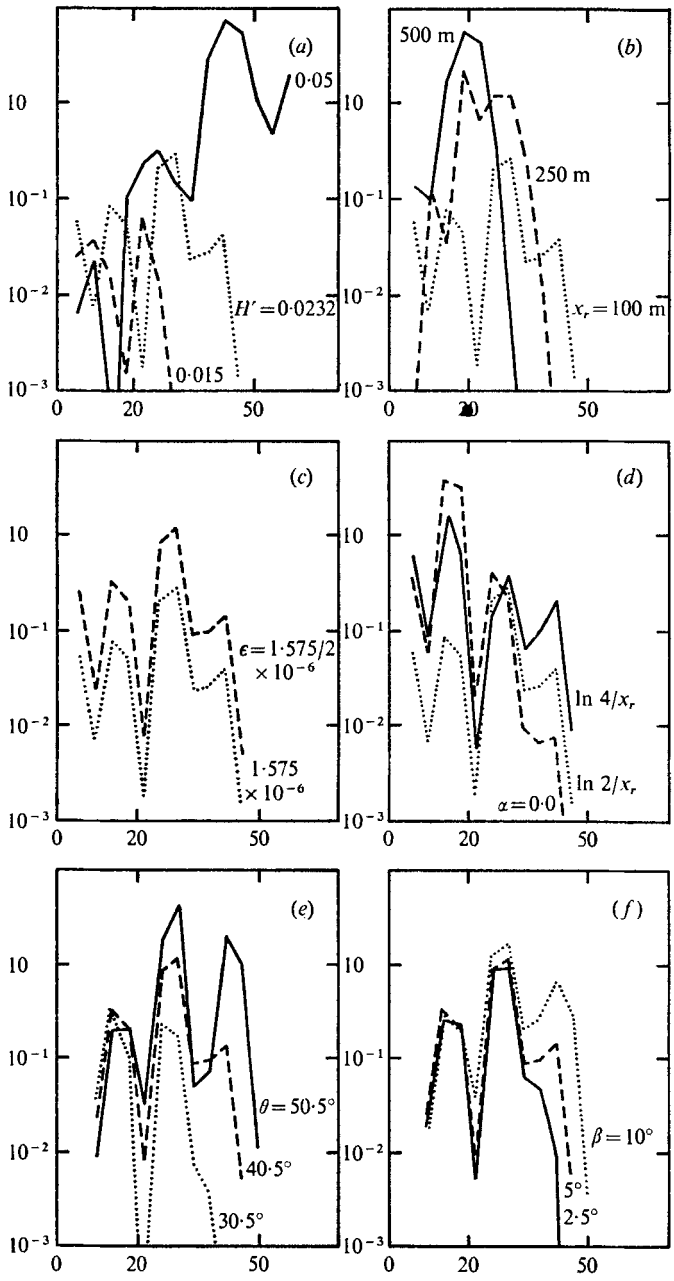

FIGURE 4. Effects of individual coastal model parameters. Curves are linear interpolations between points computed using equation (4) and the incident wave frequency spectrum of figure 6. (*a*) $x_r = 100$ m, $\epsilon = 1{\cdot}575 \times 10^{-6}$, $\theta = 40{\cdot}5$, $\beta = 5{\cdot}0$. (*b*) $H' = 0{\cdot}0232$, $\epsilon = 1{\cdot}575 \times 10^{-6}$, $\theta = 40{\cdot}5$, $\beta = 5{\cdot}0$. (*c*) $x_r = 100$ m, $\theta = 40{\cdot}5$, $\beta = 5{\cdot}0$, $\alpha = \ln 2/x_r$. (*d*) $x_r = 100$ m, $\epsilon = 1{\cdot}575 \times 10^{-6}$, $\theta = 40{\cdot}5$, $\beta = 5{\cdot}0$. (*e*) $x_r = 100$ m, $\beta = 5{\cdot}0$, $\alpha = \ln 2/x_r$, $\epsilon = 1{\cdot}575 \times 10^{-6}/2$. (*f*) $x_r = 100$ m, $\alpha = \ln 2/x_r$, $\epsilon = 1{\cdot}575 \times 10^{-6}/2$, $\theta = 40{\cdot}5$.

frictional and scattering losses, might depend on coastal and bottom topography and hence be a function of location. But at any given spot, a fixed value of ϵ should serve under a variety of input and response conditions. This was found true at Cape Palliser, New Zealand when surf-beat energy levels varied over an order of magnitude (cases 2 and 3); the ϵ-empiricism would have allowed the model to have rough predictive value. Secondly, a long-wave energy relaxation time should be approximately ϵ^{-1} for a given coast. At Cape Palliser the empirically determined ϵ yields a relaxation time of about 1·4 days, and this is in rough agreement with actual observations (see figure 8). The model also was applied to a location on the California coast (case 1). Here a smaller dissipation value was required; it corresponds to a relaxation time of 5·5 days but we have no observations to check this value. Since the coast is longer and less rugged than in New Zealand, one might expect a longer decay time. On the other hand, incident swell conditions can change appreciably in much less than five days, so a given surf-beat record might be highly contaminated by energy having nothing to do with local generation. This could have been true on the occasion we examined, in which case the computed ϵ is too small, and the implied decay time too large. More study and observations are needed on this point. However, the New Zealand examples show that there are locations where linear dissipation and the empirically determined rates have some value in representing reality.

Number of edge wave modes used

The transfer function in equation (4) contains a sum over all edge wave modes. Complexity of numerical evaluation increases rapidly with the number of modes included, so there is motivation to truncate the series at a small number of terms. Munk, Snodgrass & Gilbert (1964) found that edge wave energy observed along the coast of Southern California was concentrated in the two gravest modes. Here we have included the three gravest modes; their individual contributions to the total computed spectra are shown in figures 7 and 11. Although our computations seem reasonably satisfactory with the exclusion of higher modes, and although the cited observations did not reveal them on the occasion studied, their existence and potential importance may warrant future study.

Comparison with observations

Case one: *Camp Pendleton* (*Oceanside*), *California*, 13 *November* 1962

In this example, waves from a distant storm arrive on a long, relatively straight, continental coast at a time when local weather conditions are quiet.† The measured spectrum is plotted in figure 5. The offshore islands of Santa Catalina and San Clemente provide a 'window' on this storm which defines the base direction for the incident waves. They approach the beach at 40·5° to the local normal, and this value was used in the numerical model along with an assumed wave beam width of 20°. The offshore bottom profile shown in figure 6 was

† M/Sgt. William Powers (USMC), who studied these waves, kindly provided the information on the weather, the input direction, and the spectrum itself.

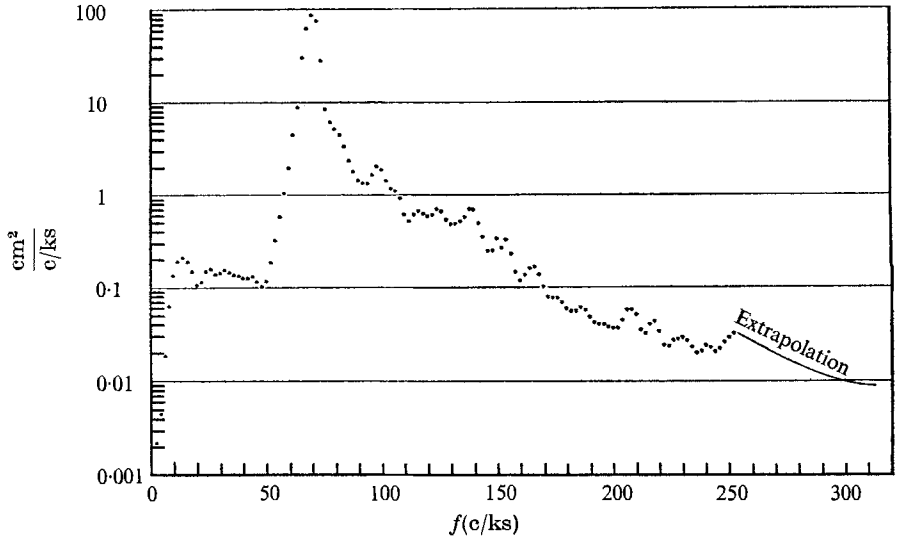

FIGURE 5. The frequency spectrum observed at Camp Pendleton, California, 13 November 1962.

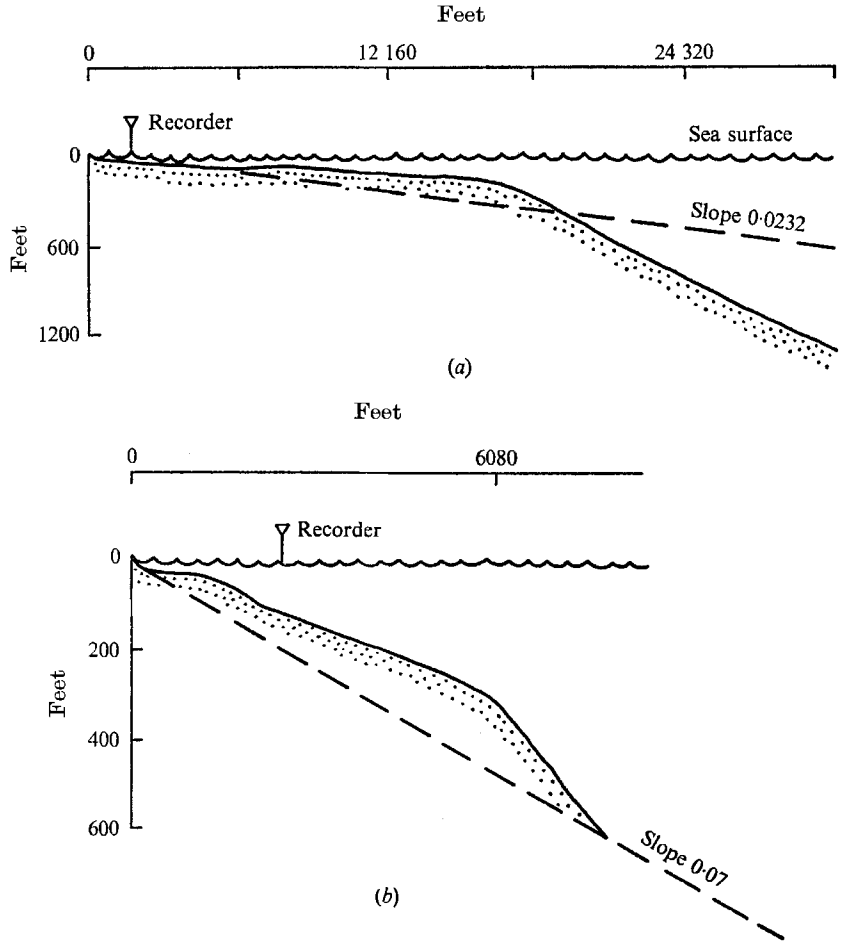

FIGURE 6. Bottom profiles at (*a*) Oceanside (Camp Pendleton), California and at (*b*) Cape Palliser, New Zealand.

approximated by an average of the two slopes present. Waves were recorded at an instrument location which Munk *et al.* (1964) describe as 500 m from shore but just seaward of the surf zone. In the model, the recorder was assumed to be 100 m outside the breaker line, with the incident swell amplitudes increasing exponentially by a factor of three between the recorder and the breaking point. The friction coefficient was set at $2{\cdot}1 \times 10^{-6}\,\mathrm{sec}^{-1}$ to produce general agreement between computed and observed surf-beat energy levels.

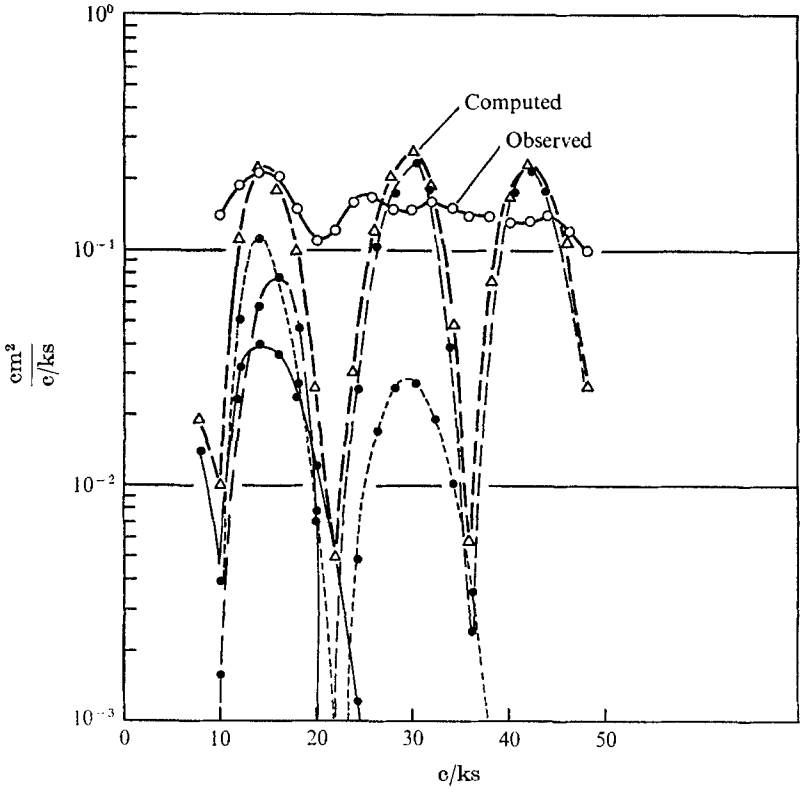

FIGURE 7. Computed and observed surf-beat spectra; Oceanside, California, 13 November 1962. $H' = 0{\cdot}0232$, $x_r = 100$ m, $\epsilon = 2{\cdot}1 \times 10^{-6}$ sec^{-1}, $\alpha = \ln(3)/x_r$, $\theta = 40{\cdot}5°$, $\beta = 20{\cdot}0°$. Mode: —, 1; - - -, 2; – –, 3.

With the above parametric values, evaluation of equation (4) produces a spectrum not unlike what was observed (figure 7). However, conclusions are hard to draw from this isolated example. The parametric values employed do not seem unreasonable, but the selection of an 'effective' recorder location and an energy dissipation rate is somewhat arbitrary and leaves room to 'tune' the model. However, experiments with parameter changes show that the model is not in a highly critical state of fine tuning; 10 % variations from the values used here would not drastically alter the results (see figure 4, which is based on the present case).

Case one illustrates that non-linear wave interaction is not completely unreasonable as a mechanism for generating surf beat. However, as mentioned in a

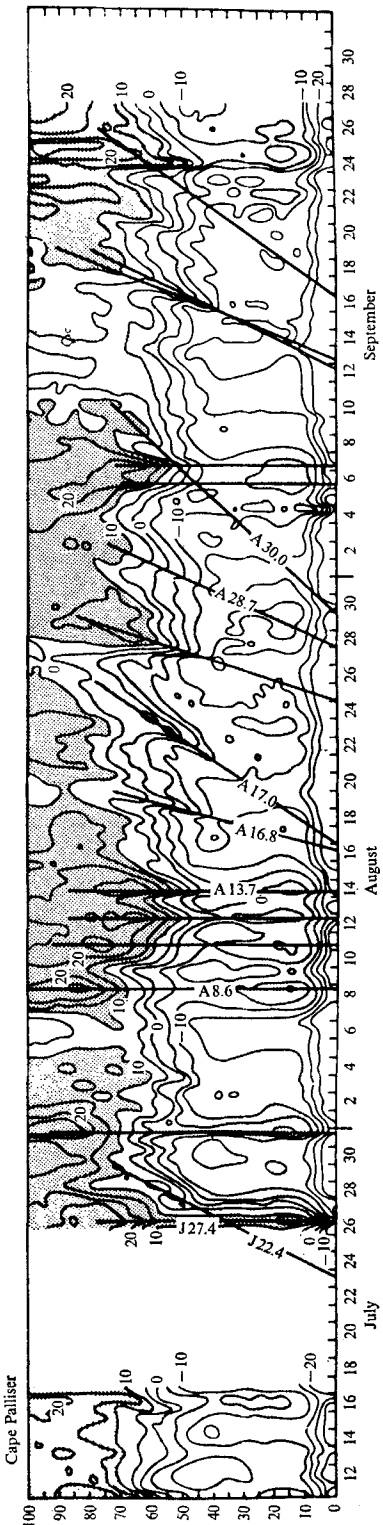

FIGURE 8. Spectral energy observed at Cape Palliser as a function of frequency and time. (From Snodgrass *et al.* (1965), by permission.)

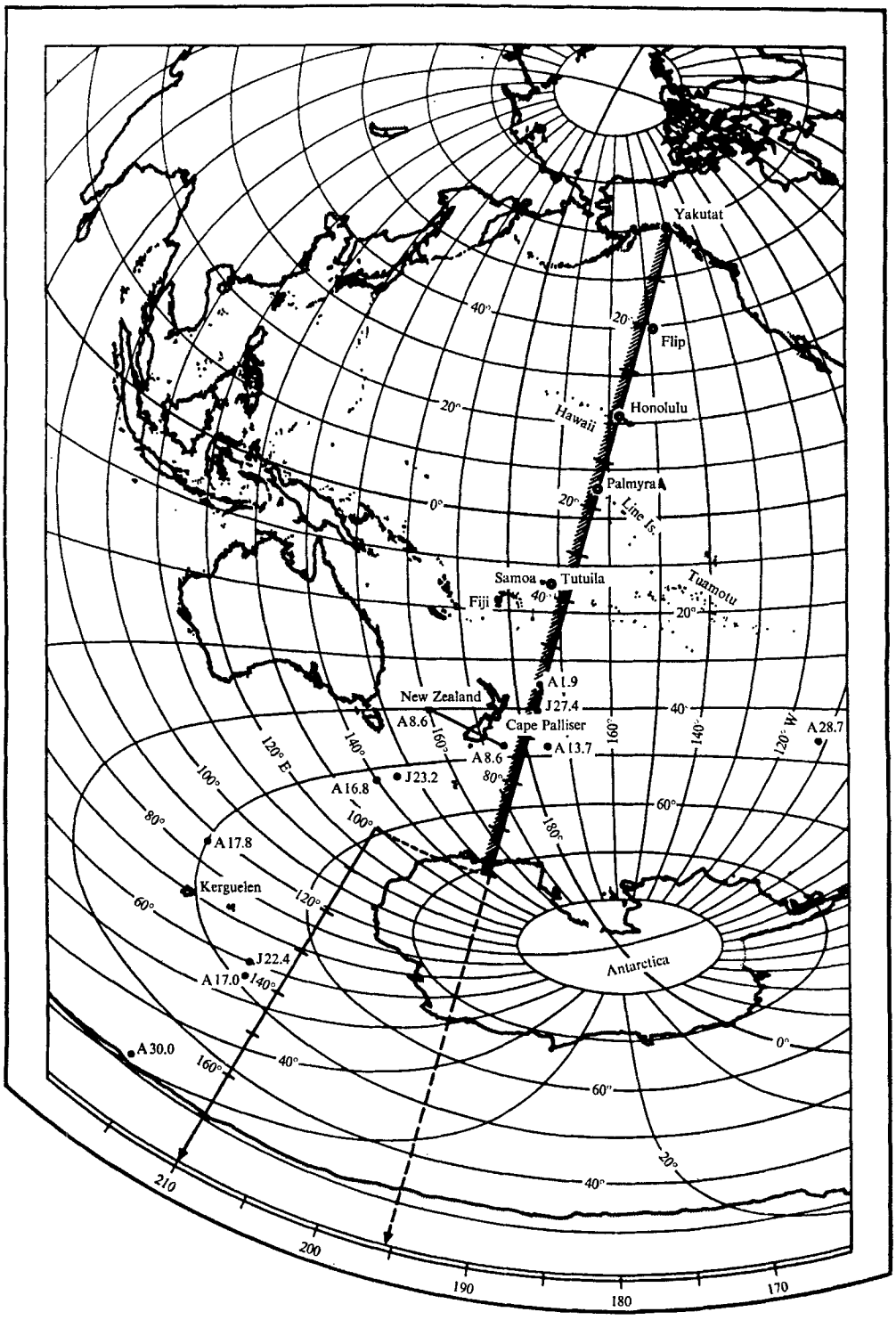

FIGURE 9. Great-circle chart based on Honolulu, showing storm locations marked by dots and fractional dates (J27.4 means 27 July, 9.6 GMT). (From Snodgrass *et al.* (1966) by permission.)

previous section, we do not know whether the dissipation rate properly characterizes this coastline, and if it does, whether we are dealing with a spectrum strongly contaminated because of the 5·5 day relaxation time. It would be well to examine examples where there is independent evidence about dissipation and a chance to test the predictive value of the analysis. This is done in cases two and three.

Cases two and three: Cape Palliser, New Zealand

Two examples from Cape Palliser provide a stronger test of the analysis. In case two, the parameters are roughly set so that a typical surf-beat condition is modelled. The dissipation rate found by this process implies a long-wave relaxation time of 1·4 days, which is consistent with the observed decay time seen in figure 8. The same model is then applied to an occasion when actual surf-beat activity was unusually high, and the observed order-of-magnitude energy increase is correctly predicted over most of the frequency range involved (case three).

Several months of wave observations were taken at Cape Palliser in 1963 as part of a wave propagation study reported by Snodgrass *et al.* (1966). A plot of wave energy as a function of frequency and time (figure 8) shows several vertical ridges crossing surf-beat frequencies – each associated with a local storm. The surf-beat ridge of 14 August was chosen for the second example because it is representative of several such occurrences. On 26 July the low frequency energy ridge is anomalous (an order of magnitude higher than any other such feature observed in three months) even though the wind-wave frequency spectrum is similar to that of 14 August. This unusual condition was selected for the third example.

A bottom profile along the local normal to the depth contours (331°) is shown in figure 6 along with the slope of 0·07 chosen for the model. Since the storms of 26 July and 14 August were both quite close to Cape Palliser (see figure 9), the incident waves were probably still under the influence of the wind as they approached shore. The shapes of the frequency spectra (figures 10 and 12) indicate little dispersion. This, together with the relatively steep bottom led us to choose $\alpha = 0$, which means the incident waves underwent no appreciable shoaling transformation in their approach to the surf zone. The actual wave recorder was 740 m from the water's edge; in the model, the line representing the 'effective' outer edge of the surf zone for the entire coast was chosen 100 m inshore from the instrument.

In case two, the direction of incident wave approach (325°) was taken from the storm centre location in figure 9, and a beam width of 24° was assigned. The dissipation parameter was adjusted to $8{\cdot}26 \times 10^{-6}$, which brings the computed surf-beat spectral level into general agreement with observation. This example provides a second demonstration that non-linear wind-wave interactions could be responsible for an observed surf-beat spectrum, as seen in figure 11.

The only factor to differ appreciably between cases two and three is storm location. On 14 August the wind waves approach the coast almost straight-on (6°), whereas on 26 July they come in at a larger angle (30°). Accordingly, we take the same coastal model used in case two, and introduce the wave frequency spectrum

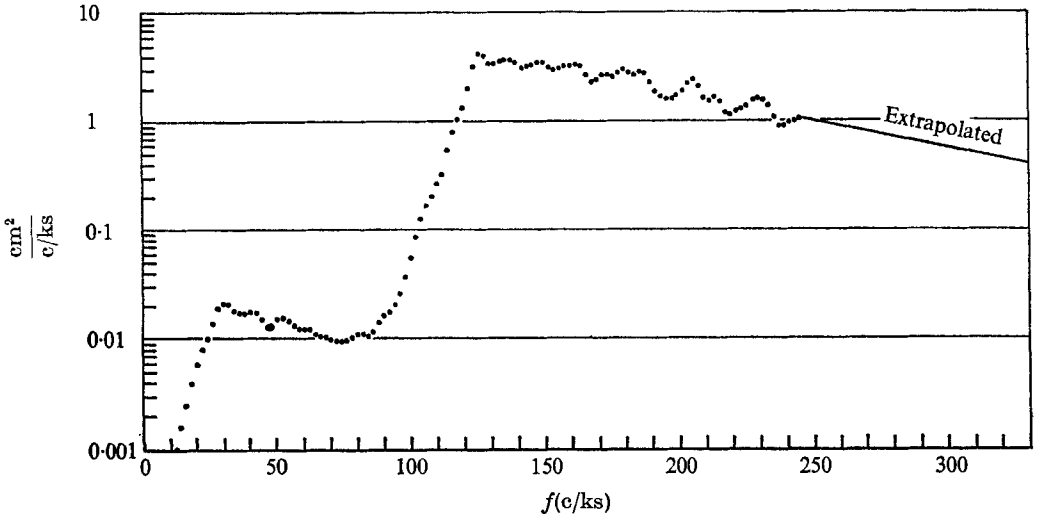

FIGURE 10. The frequency spectrum observed at Cape Palliser, New Zealand, 14 August 1963.

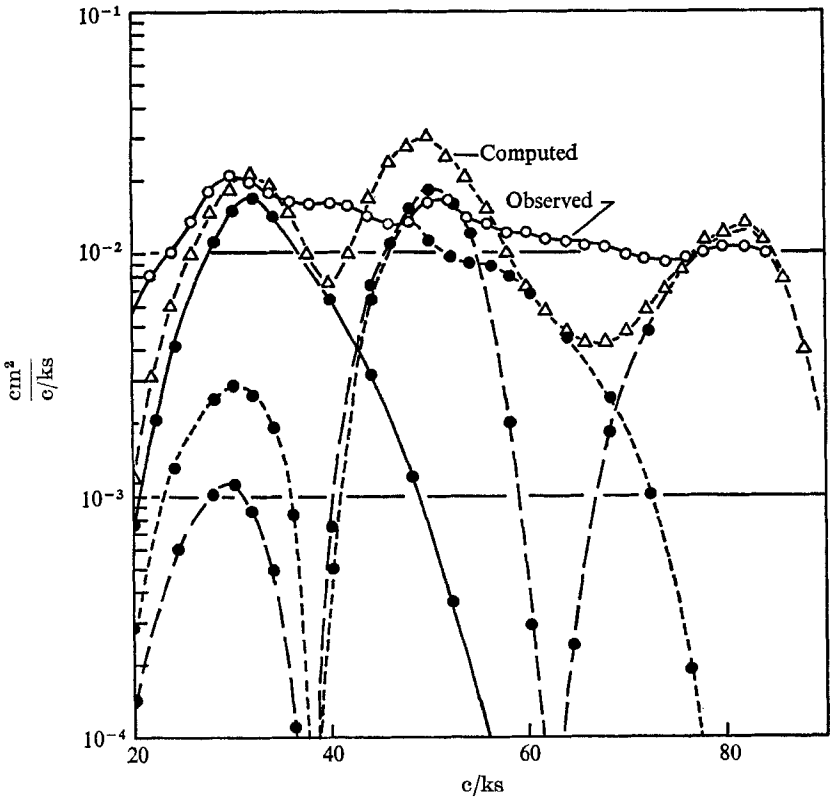

FIGURE 11. Computed and observed surf-beat spectra: Cape Palliser, New Zealand, 14 August 1963. $H' = 0{\cdot}07$, $x_r = 100$ m, $\epsilon = 8{\cdot}26 \times 10^{-6}$ sec^{-1}, $\alpha = 0$, $\theta = 6°$, $\beta = 24°$. Mode: —, 1; - - -, 2; – –, 3.

and the greater incidence angle from 26 July. The primary new feature of the observations is predicted correctly; surf-beat energy is an order of magnitude higher than on 14 August. The first of the computed curves in figure 13 shows this. Computations fall short of observed levels at lower frequencies, indicating that the model contains shortcomings. However, it would have served as a crude, qualitative predictor even in this apparently extreme case.

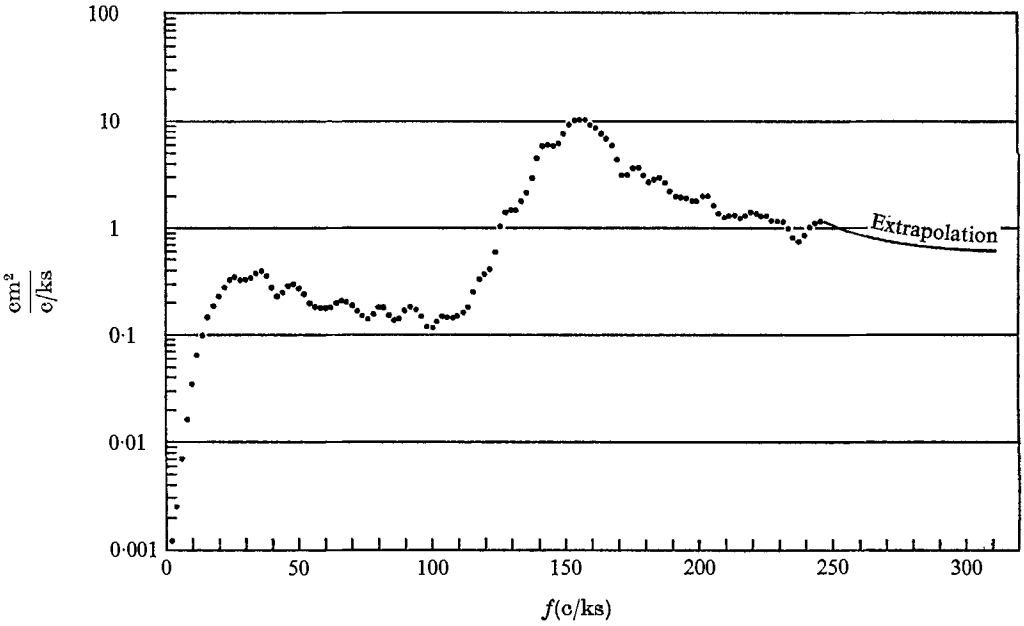

FIGURE 12. The frequency spectrum observed at Cape Palliser, New Zealand, 26 July 1963.

In the above computation, incident wave beam width was among the model parameters held constant between cases two and three, because a change would not be strictly justified by our incomplete knowledge of the directional spectra. To see the effect of an arbitrary beam width selection, we produced the second computed spectrum in figure 13 by using half the original value. The overall predictive value and shortcomings of the model remain about the same.

To illustrate further the isolated effect of storm location, we 'moved' the 26 July storm to the location of the 14 August storm and repeated the analysis. This produced marked decrease in surf-beat activity as seen in the last computed spectrum of figure 13.

The computer time required for this work was furnished and underwritten by the Statistical and Computing Center at the University of Hawaii. This is contribution no. 389 from the Hawaii Institute of Geophysics.

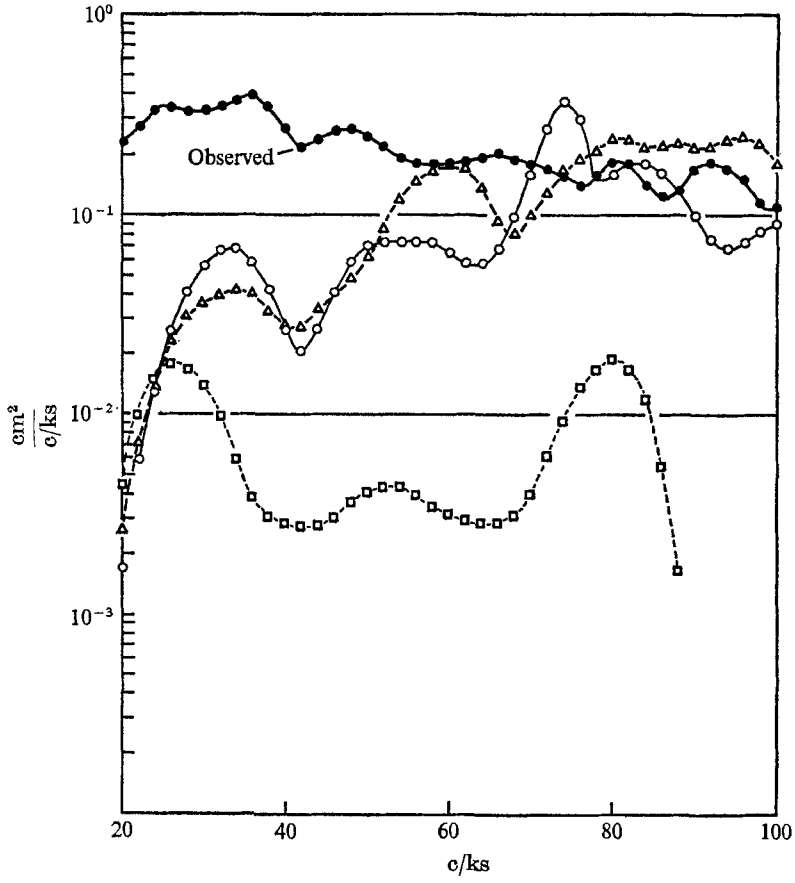

FIGURE 13. Computed and observed beat spectra:
Cape Palliser, New Zealand, 26 July 1963.

		H'	ϵ	x_r	α	θ	β
Computed	○	0·07	$8{\cdot}26 \times 10^{-6}$	100	0	30	12
	△	0·07	$8{\cdot}26 \times 10^{-6}$	100	0	30	6
	□	0·07	$8{\cdot}26 \times 10^{-6}$	100	0	6	12

REFERENCES

BIESEL, F. 1952 Equations generales au second ordre de la houle irreguliere. *La Houille Blanche*, **7**, 372–376.

HASSELMANN, K. 1961 On the non-linear energy transfer in a gravity-wave spectrum. Part 1. *J. Fluid Mech.* **12**, 481–500.

HASSELMANN, K. 1963*a* On the non-linear energy transfer in a gravity-wave spectrum, Part 2. *J. Fluid Mech.* **15**, 273–281.

HASSELMANN, K. 1963*b* On the non-linear energy transfer in a gravity-wave spectrum, Part 3. *J. Fluid Mech.* **15**, 385–398.

LONGUET-HIGGINS, M. S. & STEWART, R. W. 1962 Radiation stress and mass transport in gravity waves, with application to 'surf beats'. *J. Fluid Mech.* **13**, 481–504.

LONGUET-HIGGINS, M. S. & STEWART, R. W. 1964 Radiation stress in water waves; a physical discussion, with applications. *Deep Sea Res.* **11**, 529–562.

MUNK, W. H. 1949 Surf beats. *Trans. Am. Geophys. Union*, **30**, 849–854.

MUNK, W. H., SNODGRASS, F. E. & GILBERT, F. 1964 Long waves on the continental shelf: an experiment to separate trapped and leaky modes. *J. Fluid Mech.* **20**, 529–554.

SNODGRASS, F. E., GROVES, G. W., HASSELMANN, K. F., MILLER, G. R., MUNK, W. H. & POWERS, W. H. 1966 Propagation of ocean swell across the Pacific. *Phil. Trans. Roy. Soc.* A **259**, 431–497.

STOKER, J. J. 1957 *Water Waves.* Interscience.

TUCKER, M. J. 1950 Surf beats: sea waves of 1 to 5 min period. *Proc. Roy Soc.* A **202**, 565–573.